

## THORAX IMAGING USING TWO-DIMENSIONAL ELECTRICAL IMPEDANCE TOMOGRAPHY: A NOVEL METHOD FOR ANOMALY DETECTION BY SENSITIVITY DISTRIBUTION ANALYSIS.

Linahtadiya Andiani , Endarko

Physics Department, Institut Teknologi Sepuluh Nopember, Kampus ITS Sukolilo-Surabaya 60111, Indonesia

### ARTICLE INFO

#### Article history:

Received 1 April 2019

Revised 06 June 2019

Accepted 25 June 2019

#### Keywords:

Anomaly, EIT, Sensitivity  
Distribution, Medical Imaging,  
Thorax

### ABSTRACT

Electrical Impedance Tomography (EIT) is a non-invasive medical imaging technique which estimates the electrical impedance distribution within tissue. The basic principle of EIT is a mapping of the impedance distribution (tomography) using the measurement of some passive electrical properties of tissue named bioimpedance. The study aimed to assess the performance of the EIT system in detecting an anomaly in thorax imaging with varying different frequencies, by analysis of sensitivity distribution. Sensitivity distribution was visualized using COMSOL Multiphysics simulation in a human thorax represented as an elliptic cylinder phantom consisting of an inhomogeneous medium within and without an anomaly represented by a sphere. Current density distribution was collected for sensitivity analysis using the neighboring method with current injection at 1 mA for each pair of electrodes with frequencies 70, 100, and 130 kHz. Results indicate that the modeled two-dimensional EIT detected changes in the inhomogeneous media with and without anomaly inside the modeled thorax phantom very well.

© EuroMediterranean Biomedical Journal 2019

### 1. Introduction

In Thoracic imaging remains one of the most complicated sub-specialties of thorax diagnostic radiology (1). Modalities available for imaging thorax diseases include chest X-ray, computed tomography (CT), thoracic ultrasound, and nuclear medicine (2, 3). Electrical Impedance Tomography (EIT) is a non-invasive medical imaging technique based on tomographic imaging in which a current is applied to the body surface through contact electrodes, and the resulting surface voltages are used in the reconstruction of images. It is a new safe methodology for use in medical applications because it does not use harmful radiations (4).

Tomographic imaging is a diagnostic modality that gives the doctor a 2D cross-section view of a patient's body (5).

The basic principle of EIT is a mapping of the impedance distribution (tomography) from the measurement of some passive electrical properties of tissue named bioimpedance (6). Electrical impedance in body tissues is a function of variables such as cell geometry, organ geometry, and ion concentrations, so it is easy to imagine that sensitivity to different changes in these variables may be detectable. This sensitivity imaging is used in the reconstruction of an image from EIT (7). The sensitivity distribution from the current density of the system is affected by the layers of tissue and the dimension of electrodes.

The quality of the EIT image is dependent on the dimension of electrodes, which is adapted to the condition of tissue that will be imaged (8).

Sensitivity distribution of an impedance measurement gives a relation between the measured impedance  $Z$  change caused by a given conductivity distribution change. If conductivity change is not involved, the measured impedance can be calculated using equation (9):

$$Z = \int_v \frac{1}{\sigma} \mathbf{J}_{LE} \cdot \mathbf{J}_{LI} dv \quad (1)$$

Where  $\mathbf{J}_{LE}$  and  $\mathbf{J}_{LI}$  are the current density fields associated with the current injection and voltage measurement leads. This equation gives the contribution from each volume to the total  $Z$ , and the dot product of the two fields expresses the sensitivity to conductivity changes throughout the volume conductor (9).

Through sensitivity distribution analysis, we can evaluate the performance of the EIT system in medical imaging. The proposed study investigated the sensitivity distribution analysis of 16 electrodes of a two-dimensional EIT system in the detection of an anomaly in thorax imaging with varying different frequencies. Sensitivity distribution of EIT system is visualized using an elliptic cylinder phantom that represents a human thorax which consists of inhomogeneous media.

The anomaly media represented by a sphere (anomaly) and placed inside inhomogeneous media was also used to investigate the sensitivity distribution.

**2. Methods**

**Modelling**

The geometry models in this study were the geometry of the human thorax and the geometry of the electrode of the EIT system. All design geometries were created using COMSOL Multiphysics. Design parameters for the geometry of the human thorax, which was represented as an elliptic cylinder phantom, used the average circumference of a grown man’s thorax, which is around 1.10 m. The electrode with dimensions of  $2 \times 2 \text{ cm}^2$  with 16 pieces was used to the modeled two dimensional-EIT. The sixteen electrodes were placed along the side of the phantom’s surface. This was due to the limitations of the software which cannot detect two adjacent geometries.

The fabricated phantom with the layers of thorax tissue was made to represent the inhomogeneous media in the geometric phantom. The modeled layers assembled from outside to inside are skin dry with a thickness 0.01 m, muscle with a thickness 0.025 m, bone with a thickness 0.015 m, pleura with a thickness 0.02 m and lung with a diameter 0.15 m placed at coordinates (0.09;0;0) and (-0.09;0;0). In Figure 1, the geometric design represents the inhomogeneous media in the phantom without an anomaly. Meanwhile, for the geometric design with an anomaly is shown in Figure 2. The anomaly is represented as a right superior mediastinal disease mass which takes the form of a sphere in geometric phantom with a radius 0.0125m placed at coordinates (0,0275;0;0,045). The disease has been successfully detected using chest x-ray, CT, and MR [2,10,11].

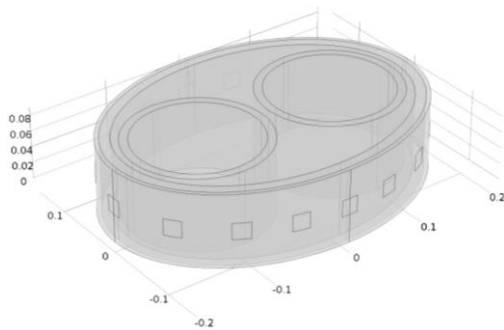


**Figure 1. The geometric design of thorax phantom without an anomaly.**

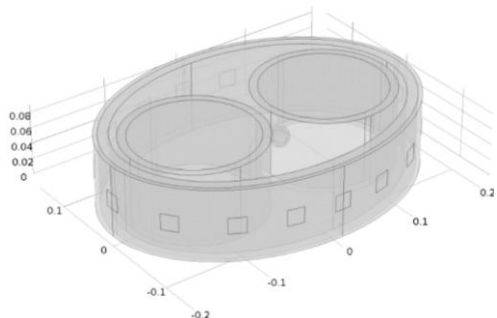


**Figure 2. The geometric design of thorax phantom with an anomaly.**

**Simulation**

The simulation stage was performed using the theoretical approach of electrical current. All physical parameters used in the study were simulated using COMSOL Multiphysics with appropriate subdomain setting, boundary setting, the solver parameter, and free mesh parameter. The physical parameters and the subdomain setting stage will be used on the designed geometry and the setting of the material type, respectively. The relative permittivity  $\epsilon_r$  and electrical conductivity  $\sigma$  for varying different tissues used in this study are summarized in Table 1.

Material	Relative Permittivity	Electrical Conductivity ( $\text{Sm}^{-1}$ )
Copper	1	$5.998 \times 10^7$
Skin Dry	1131.7	$2.1417 \times 10^{-4}$
Muscle	15521	0.34488
Bone	374.18	$2.8959 \times 10^{-3}$
Pleura	98.837	1,5
Lung Inflated	9111.3	$9.7131 \times 10^{-2}$
Anomaly	5489.3	0.53134

**Table 1. Physical parameters for different tissues in a thorax phantom.**

The measured data was performed using the neighboring method with the injected current through adjacent electrodes, and the measured voltage was recorded successively from all other adjacent electrode pairs without the pairs containing one or both the current electrodes as shown in Figure 3. The neighboring method shows a high sensitivity distribution near the electrode of the current source (12).

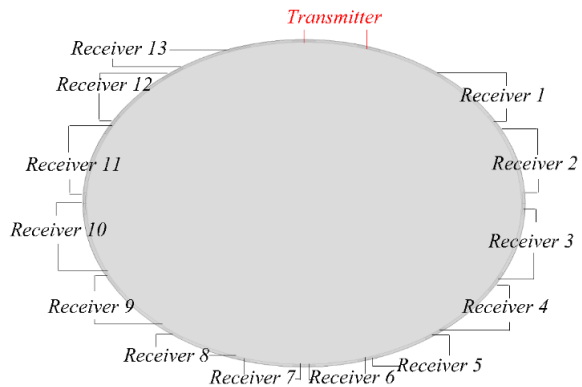


**Figure 3. Electrode boundary setting of EIT system for the first stimulation port.**

Meanwhile, the accuracy of the simulation data was achieved by setting the standard size on the free mesh parameter. The independent measurements using neighboring method for 16 electrodes produced 104 data. The measurement number could be described as a dimension’s column vector of boundary voltage and was obtained after a cyclic stimulation and measurement.

In the solver stage, the parameter is set to regulate the simulation parameters related to the physics and study stage. The purpose of this condition was to obtain the current density distribution, so in this study, we used the electrical current (ec) as the physics parameter and stationary as the study parameter. The current density values were obtained by gridding method with 32 voxels for X-axis.

**Data Iteration**

Data iteration stage is performed to obtain the current density values for each looping of the transmitter, which connected to the current source 16 times. The iteration results were used to get the sensitivity distribution of the EIT system.

**Data Processing**

The processing of iterated results of the current density data is performed to obtain the sensitivity distribution of the EIT system. The sensitivity  $S$  for current injection  $I$  can be calculated using (9):

$$S = \frac{(J_{x1}J_{x2})+(J_{y1}J_{y2})+(J_{z1}J_{z2})}{I^2} \quad (2)$$

where  $J_1$  and  $J_2$  are the current density associated with the current injection or transmitter and receiver.

In this study, the abdomen domain was divided into 32768 elements. The sensitivity distribution can be illustrated using the mean value of 104 sensitivity data in each finite element after iteration, and can be calculated using the equation as follows (13):

$$S_{avg} = \frac{1}{104} \sum_{i=1}^{104} S_{i,j} \quad (3)$$

**3. Results**

**Sensitivity Characteristic of EIT**

The sensitivity distribution generated by the EIT system on the modeled thorax phantom was conducted with various geometric conditions. In the first simulation, we proposed the thorax phantom model without anomaly, and in EIT 16 electrodes modeled in inhomogeneous media. The injected current was at 1 mA with the frequency of 70 kHz. The results generated 32 image slices with a distance between slice is 0.005625 m and the thickness of the slice is  $0.088 \times 10^{-3}$  m.

In addition, Figure 3 shows the sensitivity distribution of the first stimulation port in X-axis for the elliptic cylinder phantom of inhomogeneous without anomaly.

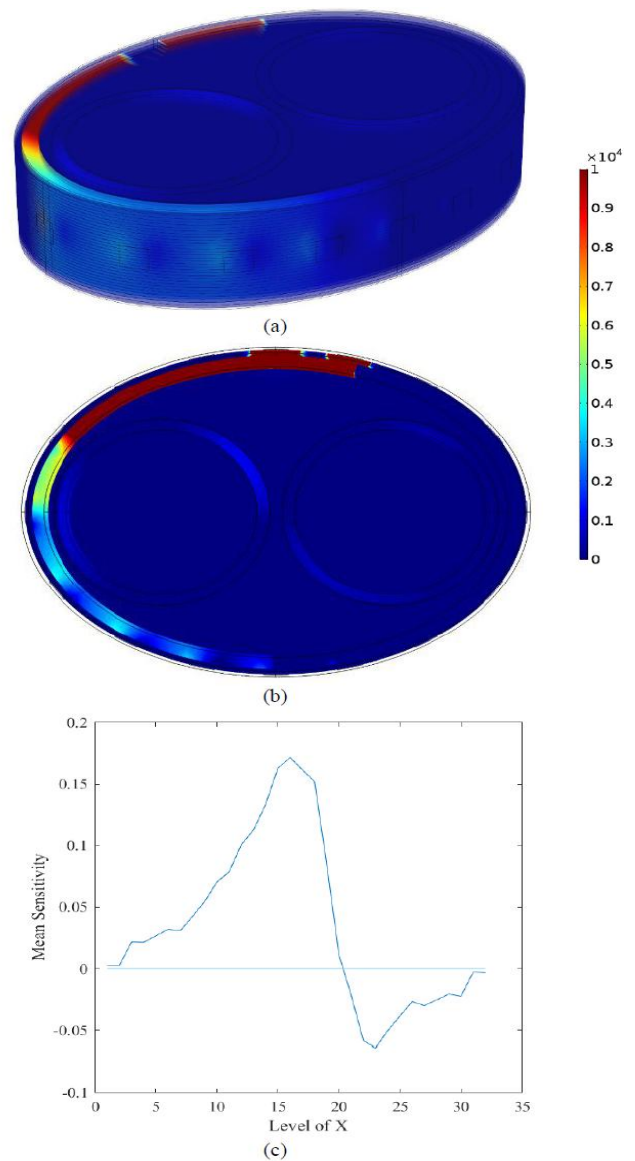
Figure 4a shows the sensitivity distribution along X-axis from the simulation for 32 slices, and Figure 4b shows the center of the slice, which is closed to transmitter electrodes. In these figures, the red color indicated high sensitivity, whereas the blue color indicated the low sensitivity. The sensitivity equals current density, and the current density also equals electric current flow. The red regions represented the position of the injected current in the pair of electrodes and the area nearest to the injected the electrodes.

Figure 4c shows the mean sensitivity graph from data processing as a function of the measurement points in the X-axis. The peak of the sensitivity distribution graph revealed that high sensitivity was achieved in the position of the injected current source. These results are in accordance with the previous study conducted by Grimnes et al., they reported that at high sensitivity, an object could be detected as very well in the region (6).

In Figure 4c it is also revealed that the electrical properties of tissue can also influence the sensitivity distribution. This is indicated by the color degradation in the muscle layer, which has high electrical conductivity and the blue color in the other layers which have low electrical conductivity.

This results is similar to the study conducted by Shuvo et al. They used five cylindrical layers with different conductivity values, the results showed that the high sensitivity distribution only occurred in the muscle layer with high electrical conductivity while the color distribution in other layers is blue which states a low sensitivity (8). The fact also corresponds to Ohm's law that electrical conductivity is inversely proportional to current density.

In the second simulation, we proposed the modeled thorax phantom with the anomaly. The proposed study was to evaluate the effect of an anomaly on the sensitivity distribution of EIT. Figure 5 shows the sensitivity distribution of the first stimulation port along X-axis for the inhomogeneous elliptic cylinder phantom with the anomaly.



**Figure 4. Sensitivity distribution along X-axis of the first stimulation port for the elliptic cylinder measurement in a homogeneous media without anomaly from the simulation for (a) 32 slices, (b) 16<sup>th</sup> slice, and (c) the mean sensitivity along X-axis from the data processing.**

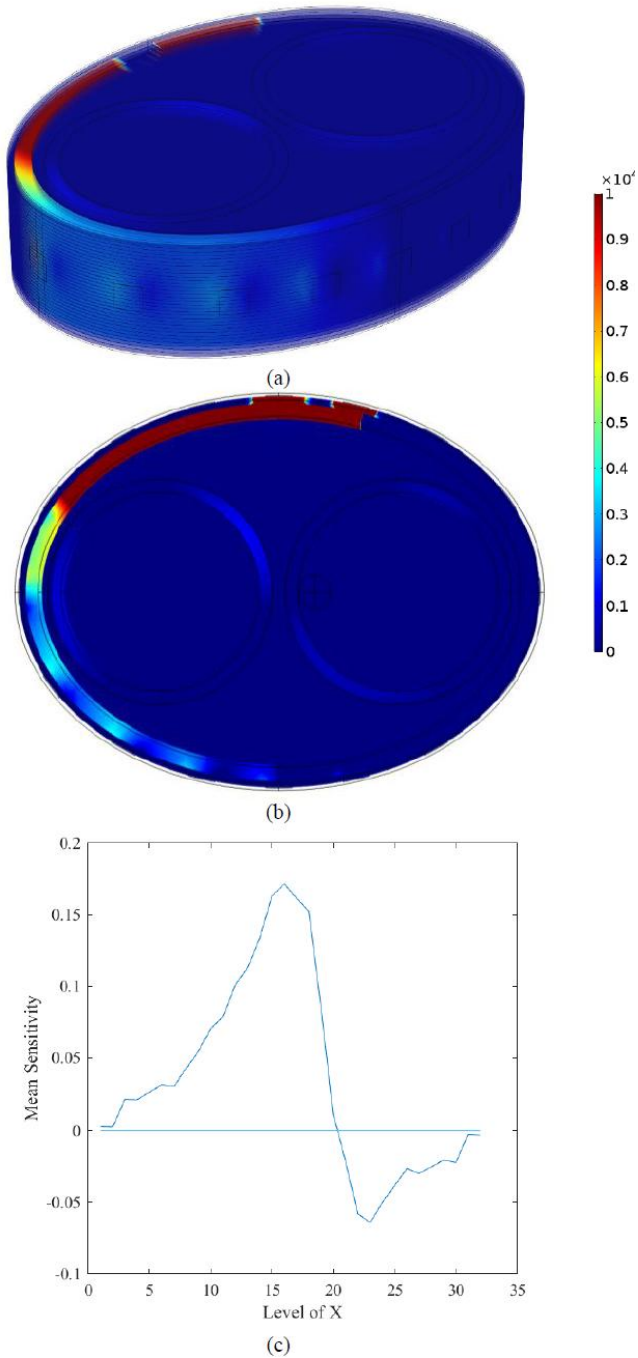


**Figure 5. Sensitivity distribution along X-axis of the first stimulation port for the elliptic cylinder measurement in a homogeneous media with anomaly from the simulation for (a) 32 slices, (b) 16<sup>th</sup> slice and (c) the mean sensitivity along X-axis from the data processing**

The results showed that the sensitivity distribution resulting in the modeled thorax phantom with the anomaly compared to the sensitivity distribution without anomaly is not significant. This is due to the fact that the injected current source has shallow penetration capability inside the phantom because of its low frequency(6).

**Anomaly Detection using Variety Frequencies**

In order to detect anomaly inside the modeled thorax phantom, we proposed the use of frequencies higher than 70 kHz. In this study, the frequencies of 100 and 130 kHz were used to detect the existence of anomalies inside the modeled thorax phantom. The input current was maintained at 1 mA for all frequencies.

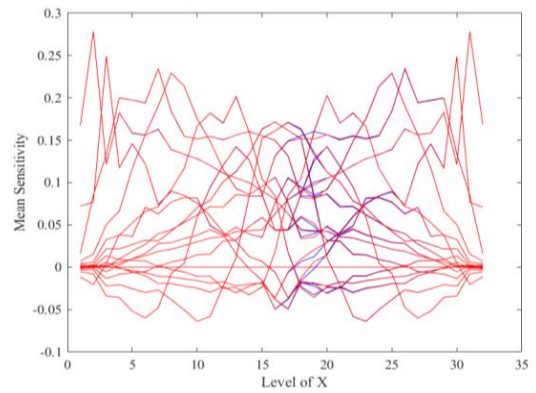


**Figure 6. Sensitivity comparison along X-axis at frequency 70 kHz for inhomogeneous media with and without anomaly**

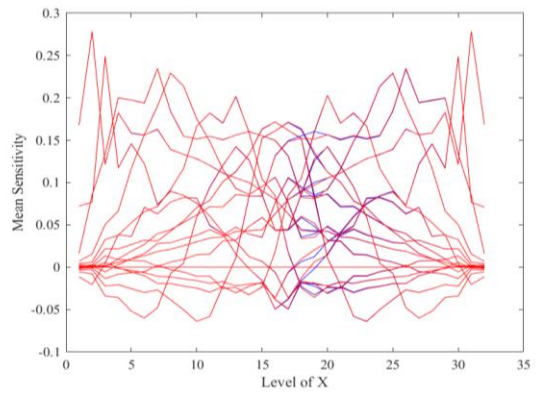


**Figure 7. Sensitivity comparison along X-axis at frequency 100 kHz for inhomogeneous media with and without anomaly**

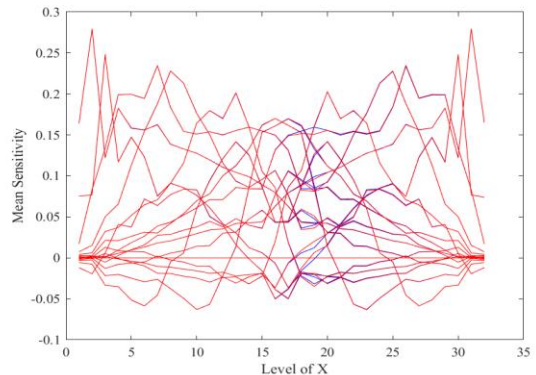


**Figure 8 - Sensitivity comparison along X-axis at frequency 130 kHz for inhomogeneous media with and without anomaly**

The sensitivity distribution of the EIT system with different frequencies are shown in Figure 6, Figure 7, and Figure 8. These figures show a sensitivity comparison distribution pattern of inhomogeneous media without anomaly (blue line) and with anomaly (red line). The results revealed that the use of the higher frequencies could detect the anomaly inside the modeled thorax phantom. There is a clear difference between without and with the anomaly. The fact indicates that the use of the higher frequencies could cause the injected current to penetrate deeper into the phantom thorax (6). The results showed that the sensitivity distribution had a potential application for quick analysis in detecting anomaly inside the modeled thorax phantom.

#### 4. Discussion

The performance of the system to detect an anomaly was assessed by analysis of the change of sensitivity in the homogeneous and inhomogeneous media. By using sensitivity analysis, we can create a real EIT system with a sensitivity system that can be adjusted to what is needed. The performance of the system to detect an anomaly can be set by changing the output frequency of the system.

In conclusion, the present study aimed to evaluate the capability of the EIT system to detect an anomaly inside the modeled thorax phantom through the analysis of sensitivity distribution. It was shown that the EIT system with 16 electrodes and the modeled thorax phantom with and without anomaly had been successfully performed, as evidenced by the systems detecting changes in sensitivity distribution with changes in frequency in the inhomogeneous media. In addition, the use of the higher frequencies revealed that the EIT system was able to detect an anomaly inside the modeled thorax phantom. For the future development of the EIT system, it would be possible to perform sensitivity analysis using a simulation process before creating the real hardware system

#### 5. Acknowledgements

This work was supported by the Kementerian Riset Teknologi Dan Pendidikan Tinggi Republik Indonesia (RISTEK-DIKTI) and the Institut Teknologi Sepuluh Nopember (ITS) Surabaya under the Postgraduate Research Grant 2018 (No. 971/PKS/ITS/2018).

#### References

- Parker MS, Chasen MH, Paul N. Radiologic signs in thoracic imaging: case-based review and self-assessment module. *AJR Am J Roentgenol.* 2009 Mar;192(3 Suppl):S34-48.
- Skinner S. Guide to thoracic imaging. *Aust Fam Physician.* 2015 Aug;44(8):558-62.
- Williamson JP, Grainge C, Parameswaran A, Twaddell SH. Thoracic Ultrasound: What Non-radiologists Need to Know. *Curr Pulmonol Rep.* 2017;6(1):39-47.
- Andiani L, Endarko, Al Huda M, Taruno WP. A novel method for analyzing electric field distribution of electro capacitive cancer treatment (ECCT) using wire mesh electrodes: A case study of brain cancer therapy. *EuroMediterranean Biomedical Journal* 2017; 12(38):178-183
- Sarode V, Patkar S, Cheeran AN. Comparison of 2-D Algorithms in EIT based Image Reconstruction. *Int J Comput Appl.* 2013 May;69(1).
- Grimnes S, Martinsen OG. *Bioimpedance and Bioelectricity Basics* Third Edition. London: Elsevier Ltd; 2015.
- Pettersen F, Høgetveit JO. From 3D tissue data to impedance using Simpleware ScanFE + IP and COMSOL Multiphysics – a tutorial. 2011;2:13–32.
- Shuvo OI, Islam MN. Sensitivity Analysis of the Tetrapolar Electrical Impedance Measurement Systems Using COMSOL Multiphysics for the non-uniform and Inhomogeneous Medium. 2016; 64(1):7–13. Available from: <https://www.researchgate.net/publication/304574700>
- Kauppinen P, Hyttinen J, Malmivuo J. Sensitivity Distribution Visualizations of Impedance Tomography Measurement Strategies. *Int J Bioelectromagn.* 2006 ; 8(1): 63-71
- Camera L, Severino R, Faggiano A, Masone S, Mansueto G, Maurea S, Fonti R, Salvatore M. Contrast enhanced multi-detector CT and MR findings of a well-differentiated pancreatic vipoma. *World J Radiol.* 2014 Oct 28;6(10):840-5.
- Corvino A, Corvino F, Radice L, Catalano O. Synchronous mucinous colonic adenocarcinoma and multiple small intestinal adenocarcinomas: report of a case and review of literature. *Clin Imaging.* 2015 May-Jun;39(3):538-42.
- Calvo Hernando M. *Electronic Instrumentation For a 3D Electrical Impedance Tomography Application.* [Finland]: Tampere University of Technology; 2015.
- Yu H, Ren S, Dong F. Sensitivity-Controlled Electrical Impedance Tomography for Abdomen Lesion Imaging. 37th Chinese Control Conf. 2018; 4091–5.